



LAWRENCE  
LIVERMORE  
NATIONAL  
LABORATORY

# Searching for Optimal Mitigation Geometries for Multilayer High Reflector Coatings

S. R. Qiu, J. E. Wolfe, A. M. Monterrosa, M. D. Feit, T. V. Pistor, C. J. Stolz

July 30, 2010

Applied Optics

## **Disclaimer**

---

This document was prepared as an account of work sponsored by an agency of the United States government. Neither the United States government nor Lawrence Livermore National Security, LLC, nor any of their employees makes any warranty, expressed or implied, or assumes any legal liability or responsibility for the accuracy, completeness, or usefulness of any information, apparatus, product, or process disclosed, or represents that its use would not infringe privately owned rights. Reference herein to any specific commercial product, process, or service by trade name, trademark, manufacturer, or otherwise does not necessarily constitute or imply its endorsement, recommendation, or favoring by the United States government or Lawrence Livermore National Security, LLC. The views and opinions of authors expressed herein do not necessarily state or reflect those of the United States government or Lawrence Livermore National Security, LLC, and shall not be used for advertising or product endorsement purposes.

# Searching for optimal mitigation geometries for multilayer high reflector coatings

S. Roger Qiu<sup>a\*</sup>, Justin E. Wolfe<sup>a</sup>, Anthony M. Monterrosa<sup>b</sup>, Michael D. Feit<sup>a</sup>,  
Thomas V. Pistor<sup>c</sup>, Christopher J. Stolz<sup>a</sup>

<sup>a</sup>Lawrence Livermore National Laboratory, 7000 East Avenue, Livermore, CA 9455. Phone:  
(925) 422-1636 Fax: (925) 423-0792

<sup>b</sup>Department of Nuclear Engineering and Department of Materials Science & Engineering,  
University of California, Berkeley, CA 94704

<sup>c</sup>Panoramic Technology Inc., 2039 Shattuck Ave., Suite 404, Berkeley, CA 94704

\*Corresponding author: e-mail address: qiu2@llnl.gov

Growing damage sites on multilayer high reflector coatings can limit mirror performance. One of the strategies to improve damage resistance is to replace the growing damage sites with pre-designed benign mitigation structures. To determine the optimal mitigation geometry, the finite difference time domain method was used to quantify the electrical field intensification within the multilayer, at the presence of different conical pits. We find that the optimal mitigation structure of conical pits should either possess a shallow cone angle of no more than 30° or have the cone angle matched to the angle of incidence of the incoming wave.

**OCIS codes:** (310.0310) Thin film, (230.7370) Waveguide, (140.3330) Damage.

## 1. Introduction

High dielectric constant multilayer coatings are commonly used on mirrors for high peak power laser systems because of their high laser damage resistance. For example, in mirrors used in the National Ignition Facility, silica-hafnia multilayer coatings are coated on BK7 substrates by e-beam physical vapor deposition. During the deposition process, physical defects are often formed within the multilayer film. These physical defects include highly absorbing nano-clusters at the near surface region of the film and solid inclusions in the bulk film. In addition, some substrate surface flaws (e.g. scratches) can also cause films to grow defectively. Earlier studies [1-4] have shown that all these defect types can cause laser-induced damage on the coated layers even at a fluence that is much lower than that of the operation. Some of these initiated damage sites, although rare in comparison to the total number of defects within the film, can grow under further laser irradiation, and thus eventually limit the mirror performance and lifetime.

In parallel with attempts to increase film quality by suppressing the number of defects within the coating layers, other active efforts have also been made to enhance mirror performance and lifetime by increasing the damage threshold upon laser irradiation. One of the strategies is to first initiate the damage precursors at fluencies below the operational fluence, and then replace the initiated damage sites with a pre-designed benign mitigation structure [5] with a much higher damage threshold. These mitigation structures can be created by multiple techniques including femtosecond laser machining, single crystal high-speed diamond machining, and magnetorheological finishing [5-7]. In fact, our earlier study of creating rationally designed features utilizing femtosecond laser machining [5] has shown an increase in the laser damage threshold, from  $15 \text{ J/cm}^2$  to  $40 \text{ J/cm}^2$  for light at 1064 nm, with a 3ns pulse length. However, to

maximize the effort, one must have a rational means to search for an optimal mitigation structure that can routinely yield a higher laser damage threshold than the operational fluence.

A combination of theoretical and experimental efforts has been put forth to determine the optimal mitigation geometry. For the theoretical effort, we have utilized the finite difference time domain (FDTD) method to quantify the electric field distribution within the coating layers in the presence of the pre-defined defects of different shapes. This approach is motivated by the belief that laser-induced damage within thin film layers is strongly correlated with electric field intensification created by the presence of interface and coating defects [8-10]. Experimentally, we utilize femtosecond laser machining to fabricate mitigation structures suggested by the simulation work and to further examine the manufactured feature for damage resistance as well as to validate the theoretical predication.

In this paper, we report on results examining conical pits as potential mitigation geometries. To realistically mimic the true mitigation features, the theoretical simulation was performed as a 3-D structure. Furthermore, the impact of polarization on multilayer damage resistance was also investigated. Overall, results of electrical field intensification obtained through 3-D simulation are consistent with those obtained previously through 2-D simulation [11]. For a conical a pit-bearing multilayer coating, the light intensification is usually smaller for pits with shallow cone angles ( $< 30^\circ$ ). Alternatively, field intensification is minimized when the cone angle and incident angle are matched. Simulation results were validated by laser-induced damage. Our results suggest that conical pits can be used as potential mitigation structures provided the following

criteria are satisfied: the cone angle is no greater than  $30^\circ$  or the cone angle matches with the application angle of incidence.

## 2. Method

A commercially available software code TEMPESTpr2 employing the FDTD method is used to solve Maxwell's equations within a 3-D domain containing conical pit structures. A detailed description of this code can be found elsewhere [12]. For the current application, the algorithm simulates the scattering of an electromagnetic plane wave that propagates through a defective multilayer topography as shown in Fig. 1. The simulation domain is a 3-D rectangular and gridded uniformly. The periodic boundary conditions (PBC) are applied in the horizontal direction, while the Berenger's perfectly matched layer (PML) absorbing-boundary condition is applied in the vertical direction. In addition, absorbing layers with median refractive indices were also manually added to the outside edges of the simulation domain in the x-z plane to minimize the impact of the PBC and to prevent back reflections. The validation of the application of this code for calculating electrical field intensification for a multilayer high reflector coating is discussed in detail in reference [11].

The 3-D domain used for the current study (Fig. 1) consists of twenty-four alternating layers of hafnia (H) and silica (L) with a quarter-wave reflector design: air:L(L:H)<sup>12</sup>:glass. The refractive indices of the layers are  $n_H=1.971$  and  $n_L=1.44977$ . The physical thickness of each hafnia and silica layer is 133.56 and 181.58 nm, respectively. The total film thickness is 3963.26 nm. Due to the limitation of computation power for the 3-D simulations, the film thickness is discretized with a 7-cell per bilayer instead of the 12-cell per bilayer arrangement for the 2-D

calculation [11]. For conical pits, the cone angles range from  $0^\circ$  to  $75^\circ$  at  $15^\circ$  increments and the incident angles of the incoming wave range from  $0^\circ$  to  $60^\circ$  at  $5^\circ$  increments. For oblique incidence cases, the irradiation wavelength for the simulation was blue-shifted to maintain maximum reflectivity and proper spectral centering; the refractive indices were also replaced by the effective values to ensure the quarter wave optical thickness is satisfied throughout the simulations. The description of film thickness, wavelength, and refractive index modifications for waves impinged along off-normal directions can be found in detail in ref. [11]. The electrical field intensification strength within the domain is quantified by the normalized electrical field intensity or the square of electric field,  $|\mathbf{E}|^2$  with respect to that of the incoming wave; i.e., a value of 1 indicates no field intensification and the larger the value, the stronger the electrical field intensification.

Femtosecond laser machining is used to create conical pits of  $15^\circ$  on a 2" round BK 7 substrate [5] coated with high reflective multilayer similar to those used in the simulations. The pits are created with diameters of 0.5mm-to 1.0mm and are  $\sim 10$ - $15\mu\text{m}$  deep. The mitigation feature-bearing multilayer film is exposed to 1064nm laser with 3ns pulse length for laser-induced damage testing following the protocol described in a report [13] .

### **3. Results and Discussion**

Electrical field intensification is observed in both hafnia and silica layers. Because the damage resistance and the correlation between light intensification and damage initiation or growth of these materials are different, the simulation results are grouped by material type; i.e., hafnia and silica. The characteristics of electrical field intensification within the hafnia layers are shown in

Figs. 2-5 and those within the silica layers are shown in Figs. 6-9. In general, for both material types, the spatial distribution of the electrical field intensification is polarization-dependent and the maximum intensification is in the opposite side of the cone for s- and p-polarized light, respectively. This is true for all cone angles and angles of incidence.

### **3.1 Electrical field intensification within the hafnia layers**

The cross-sectional view of the electrical field intensification distribution within the multilayer coating is shown in Figs. 2 and 3 for both s- and p-polarized waves at the presence of a conical pit of  $15^\circ$ . When the s wave is irradiated at  $45^\circ$  off-normal to the left, the high intensification area is manifested at the right side region to the cone. However, for p-polarized light, the high intensification region is at locations on the left side of the cone. Such a difference can be easily discerned in Figs. 2 and 3. While Figs. 2 (a) and 3 (a) show the top-view of the electrical field intensification at the layer where maximum intensification resides, Figs. 2 (b) and 3 (b) show the side view of the field intensification within the film. The higher the color scale is, the larger the field enhancement. The maximum intensification for the s wave is located at the second hafnia layer from the top, but for the p wave, it is located at the top layer. The maximum intensification spot for both cases is shown by the red spot in Figs. 2 (b) and 3 (b), respectively.

To understand the general trend of the electrical field intensification in the multilayer coating with a mitigation feature, simulations were performed for different conical pits irradiated at both s- and p-polarized light at various incident angles. The maximum intensification values are summarized in Fig. 4 for all simulated conditions. Both a column plot and a surface plot were used to better display the important features of the simulated results. As shown in Fig. 4 (a), for

the s-polarized light, the maximum intensification in the hafnia layer varies in a wide range, for example from as low as 1.5 to as high as 9.5, depending on the combination of cone angle and light irradiation direction. For a given cone angle, the dependence on incident angles in most cases, can be expressed by a monotonic function. However, for a fixed angle of incidence, the dependence of the maximum intensification on cone angles is more complex and does not follow a simple trend. Another important feature exhibited in Fig. 4 (a) is that, for a cone angle of  $30^\circ$ , the magnitude of the intensification for all angles of incidence, in large, is smaller than their counterparts. A similar trend can be seen for the cone angle of  $15^\circ$ . Thus our results suggest that optimal mitigation conical pits should bear a conical angle smaller than  $30^\circ$ .

To better visualize the convoluted impact of both the cone angle and angle of incidence on electrical field intensification, the simulation results are displayed in a pseudo-3D surface plot (Fig. 4 (b)). Besides showing the information already discussed in Fig. 4(a), Fig. 4(b) displays another important feature that is, when the angle of incidence is matched with the cone angle, the least amount of field intensification is also achieved. This important feature is indicated by the blue solid line in the figure.

The simulation result for the p-polarized light (p wave) is shown in Fig. 5. Although the exact dependence on cone angle and angle of incidence may vary, the maximum intensification for the p wave exhibits similar characteristics as those from the s wave. That is, the intensification from features with cone angles smaller than  $30^\circ$ , on average, are smaller than that from larger cone angles and the intensification is minimized when the angle of incidence is matched with the cone angle. It is worthwhile to note that the magnitude of the maximum intensification for the p wave

is generally much smaller than that for the s wave. For example, at p polarization, for a feature at a  $45^\circ$  cone angle at normal incidence, the intensification maxima is only 4 compared to nearly 10 at s-polarization. Thus our simulation results suggest that the multilayer high reflector coating may be more robust against impinging p-polarized light.

### **3.2 Electrical field intensification within the silica layers**

Simulation results for the silica layers showed very similar characteristics to that of the hafnia layers in electrical field intensification. Examples of the cross-sectional distribution of the field intensification are shown in Fig. 6 for the s wave and in Fig. 7 for the p wave; both for a  $15^\circ$  cone under  $45^\circ$  irradiation off normal. The magnitude of the intensification maxima is displayed in Fig. 8 and Fig. 9 for s and p waves respectively. For instance, the location of the maximum intensification within the silica layers is at the right side of the cone for the s wave and at the left side of the cone for p wave. This is consistent with that for the hafnia layer. The only difference, however, is that for the s wave, the maximum intensification is at the first layer from the top in contrast to that at the second layer for the hafnia material. For p wave, both are at the top layer. Furthermore, judging from plots in Figs. 8 and 9, the magnitude of the intensification maxima within the silica layer is also smaller on average for shallow cone angles ( $< 30^\circ$ ) at all angles of incidence and the intensification is minimized when the angle of incidence is matched with the cone angle of the mitigation feature. The magnitude of intensification maxima is higher in general for the s wave than for the p wave.

In comparison to the hafnia layers, the maximum intensification within the silica layer is generally higher. However, for a given cone angle, the dependence of intensification on incident

angle is not as strong. These characteristics are especially apparent for lower cone angles. Earlier studies have reported that laser-induced damage sites are more often observed at the hafnia layers. Since material with less intensification is more prone to damage, our simulation results suggest that besides electrical field intensification, internal physical properties of coating materials play an important role in mirror performance.

### **3.3 Waveguide effect**

In an earlier study, we reported our observation of an interesting phenomenon where a waveguide effect was responsible for the electrical field intensification within a defective multilayer film containing a cylinder [11]. In the current work, we conduct a thorough study by examining the waveguide effect on light intensification for a series of cones under different irradiation directions. After careful analysis of the simulation data for all combinations of cone angle and angle of incidence, we find that waveguide effect is the main cause of light intensification for pits with cone angles smaller than  $30^\circ$  at all angles of incidence. The waveguide effect, however, is not observed to be the cause of the high intensification through the film for the p waves.

Since fabricated conical pits with cone angles smaller than  $30^\circ$  are one of the suggested mitigation strategies, it is beneficial to suppress the waveguide formation for the lower cone angle features. It is believed that a rough edge at the cone boundary may be able to break the coherence of light and thus eliminate the waveguide effect and light intensification. To test this hypothesis, simulations are performed for rough pits with cone angles at  $0^\circ$  and  $15^\circ$  respectively. The morphology of the rough edge was obtained by cross-sectioning the benign pits created with

femtosecond laser machining in reference [5]. Fig. 10 shows the simulated field intensity distribution within the multiple layers at the presence of a 15° smooth- (Fig. 10 (a)) as well as rough-edged (Fig. 10 (b)) cone, with light beam irradiating at 45° from the surface normal. It is apparent that waveguide patterns exist in both cases. Thus the rough edge at the cone boundary does not reduce the waveguide effect within the film. This result suggests that the irregularity of the rough edge created by micro-machining may be too small (in comparison to the beam wavelength at 1053 nm) to reduce the coherence. Future efforts are in progress to find an effective means to suppress the waveguide effect.

### **3.4. Laser damage test**

Preliminary experimental results employing laser testing show that multilayer coatings that contain mitigation conical pits of 15° have a much higher damage threshold than the non-mitigated layers. For s-polarized light irradiated at 45° from the normal, the thin film damage appears at a region near the mitigation site when laser fluence reaches to 42 J/cm<sup>2</sup>. For p-polarized light, the thin film damage threshold is 54 J/cm<sup>2</sup>. Both values far exceed the nominal damage threshold of 20 J/cm<sup>2</sup> for the non-mitigated multilayer high reflector coatings over large apertures.

The morphology of the multilayer with the conical pit mitigation feature prior to and after damage is shown in Fig. 11. Fig. 11 (a) is a top view light microscope image that displays the features within the film. The black circle represents the conical pit and the darker fuzzy region at the upper left side of the circle is the debris from the femtosecond laser machining. The morphology after s wave damage is shown in Fig. 11 (b). As highlighted by the yellow arrow,

the film at the right side of the circle shows strong delaminations and loses its smoothness due to damage. In contrary, the damaged sites under p wave are located at the left side of the circle which can be easily seen in Fig. 11 (d) (indicated by yellow arrow). Interestingly, the damaged locations under each polarization agree well with the theoretical predications as discussed in the previous sections (Figs. 2-3). To help demonstrate the resemblance, simulation results for similar light irradiation conditions to the laser damage testing are displayed in Figs. 11 (c) and (e), for the s and p waves respectively. As indicated by the yellow circles in the figures, the predicted highest intensification spot under 45° irradiation is located at the right side of the pit for the s wave and at the left side for the p wave.

In addition to the agreement between calculations and experiment in damage locations, the fluence ratio is also comparable to the intensification ratio. For example, the theoretical calculation predicts that the maximum intensification is ~3.5 for s-polarized light and 2.6 for p-polarized light. If one assumes that the laser-induced damage is directly related to electrical field intensification, the damage threshold for the s-polarized light should be less and the measured damage threshold should be proportional to the calculated maximum intensification. This in fact is what we have observed from both the experimental testing and theoretical calculation. We find that the ratio of the maximum intensification between p and s waves is at ~ 0.74 and the ratio of measured damage fluences for s and p waves is at ~ 0.78. They are essentially the same within experimental errors. In short, the agreement between the experimental and theoretical results further support the hypothesis that electrical field intensification is one of the major causes of laser-induced damage in multilayer high reflector coatings.

#### **4. Summary**

In summary, simulation utilizing FDTD method has shown that conical pits generate high electrical field intensification within the multilayer high reflector coating. The magnitude of the intensification is strongly dependent on cone angles and angle of incidence of the incoming wave. Moreover, the location of the maximum field intensification is also polarization dependent which has been confirmed by laser-induced damage testing. A waveguide effect is one of the sources for field intensification, especially for mitigation features with lower cone angles. Our results suggest that for mitigation strategies that are able to create a range of conical pit angles, the optimal pit geometry should match the pit angle with the angle of incidence. Alternatively, mitigation strategies with less angular range flexibility should resort to a 30° cone angle or less to avoid creating a waveguide structure while minimizing light intensification.

#### **Acknowledgment**

We thank Spica Technologies, Inc. for performing the laser-induced damage testing. This work was performed under the auspices of the U.S. Department of Energy by Lawrence Livermore National Laboratory under Contract DE-AC52-07NA27344 and funded in part by Laboratory Directed Research and Development Grant 09-ERD-051.

## References

1. J. DiJon, P. Garrec, N. Kaiser, and U. B. Schallenberg, "Influence of substrate cleaning on LIDT of 355 nm HR coatings," Proc. SPIE **2966**, 178-186 (1997).
2. J. DiJon, T. Poiroux, and C. Desrumaux, "Nano absorbing centers: a key point in the laser damage of thin films," Proc. SPIE **2966**, 315-325 (1997).
3. F. Y. Genin and C. J. Stolz, "Morphologies of laser-induced damage in hafnia-silica multilayer mirror and polarizer coatings," Proc. SPIE **2870**, 439-448 (1996).
4. S. H. Li, H. B. He, D. W. Li, M. Zhou, X. L. Ling, Y. A. Zhao, and Z. X. Fan, "Temperature field analysis of TiO<sub>2</sub> films with high-absorptance inclusions," Appl. Optics **49**, 329-333 (2010).
5. J. E. Wolfe, S. R. Qiu, C. J. Stolz, M. Thomas, C. Martinez, and A. Ozkan, "Laser damage resistant pits in dielectric coatings created by femtosecond laser machining," Proc. SPIE **7504**, 750405-750401 (2009).
6. P. Geraghty, W. Carr, V. Draggoo, R. Hackel, C. Mailhiot, and M. Norton, "Surface damage growth mitigation on KDP/DKDP optics using single-crystal diamond micro-machining ball end mill contouring - art. no. 64030Q," Proc. SPIE **6403**, Q4030-Q4030 (2007).
7. M. Tricard, P. Dumas, and J. Menapace, "Continuous phase plate polishing using magnetorheological finishing," Proc. SPIE **7062**, 70620V (2008).
8. P. W. Baumeister, *Optical Coating Technology* (SPIE, 2004).
9. C. J. Stolz, M. D. Feit, and T. V. Pistor, "Laser intensification by spherical inclusions embedded with multilayer coatings," Appl. Optics **45**, 1594-1601 (2006).

10. Y. Wang, Y. G. Zhang, X. Liu, W. L. Chen, and Y. Y. Li, "Analysis of laser intensification by nodular defects in mid-infrared high reflectance coatings," *Acta Phys. Sin.* **56**, 6588-6591 (2007).
11. S. R. Qiu, J. E. Wolfe, A. M. Monterrosa, M. D. Feit, T. V. Pistor, and C. J. Stolz, "Modeling of light intensification by conical pits within multilayer high reflector coatings," *Proc. SPIE* **7504**, 75040M-75041 (2009).
12. T. V. Pistor, "Electromagnetic simulation and modeling with applications in lithography," (University of California, Berkeley, Berkeley, 2001).
13. M. R. Borden, J. A. Folta, C. J. Stolz, J. R. Taylor, J. E. Wolfe, A. J. Griffin, and M. D. Thomas, "Improved method for laser damage testing coated optics," *Proc. SPIE* **5991**, A9912-A9912 (2005).

**Fig. 1.** Schematics of 3-D simulation domain showing a multilayer coating with a conical pit of  $15^\circ$  cone angle on a BK7 glass substrate. The hafnia layers are represented by the green color while the light blue color represents silica layers, the glass substrate, and cap layer.

**Fig. 2.** Electrical field intensity distribution in the hafnia layer with a  $15^\circ$  conical pit for s-polarization light irradiated at  $45^\circ$  where the highest intensification resides. The maximum intensification is located at the second hafnia layer from the top and at the right side of the cone edge which is delineated by the dotted white lines. Higher color scale value corresponds to higher field enhancement. (a) Cross section that is perpendicular to plane of incidence. (b) Cross section that is parallel to the plane of incidence. For view purpose, the image in (b) is stretched along the vertical direction.

**Fig. 3.** Electrical field intensity distribution in the hafnia layer with a  $15^\circ$  conical pit for p-polarization light irradiated at  $45^\circ$  where the highest intensification resides. The maximum intensification is located at the first hafnia layer from the top and at the left side of cone edge which is delineated by the dotted white lines. Higher color scale value corresponds to higher field enhancement. (a) Cross section that is perpendicular to plane of incidence. (b) Cross section that is parallel to the plane of incidence. For viewing purposes, the image in (b) is stretched along the vertical direction.

**Fig. 4.** Distribution of the maximum intensification within the hafnia layers in the defective multilayer coating film for various cone angles and s-polarization light irradiation at a series of incidence angles. (a) 2-D column plot. The red dotted circle indicates that a  $30^\circ$  conical pit generates the least amount of field intensification on average for all incidence angles. The color-box legend indicates the angle of incidence. (b) Contour plot. The blue line indicates that light

intensification in mitigation sites is minimized when the cone angle and the incident angle are matched. The color-box legend represents the magnitude of intensification.

**Fig. 5.** Distribution of the maximum intensification within the hafnia layers in the defective multilayer coating film for various cone angles and p-polarization light irradiation at a series of incidence angles. (a) 2D column plot. The red dotted circle indicates that a  $30^\circ$  conical pit generates the least amount of field intensification on average for all incidence angles. The color-box legend indicates the angle of incidence. (b) Contour plot. The blue line indicates that light intensification in mitigation sites is minimized when the cone angle and the incident angle are matched. The color-box legend represents the magnitude of intensification.

**Fig. 6.** Electrical field intensity distribution in the silica layer with a  $15^\circ$  conical pit for s-polarization light irradiated at  $45^\circ$  where the highest intensification resides. The maximum intensification is located at the first silica layer from the top and at the right side of cone edge which is delineated by the dotted white lines. Higher color scale value corresponds to higher field enhancement. (a) Cross section that is perpendicular to plane of incidence. (b) Cross section that is parallel to the plane of incidence. For viewing purposes, the image in (b) is stretched along the vertical direction.

**Fig. 7.** Electrical field intensity distribution in the silica layer with a  $15^\circ$  conical pit for p-polarization light irradiated at  $45^\circ$  where the highest intensification resides. The maximum intensification is located at the first silica layer from the top and at the left side of cone edge which is delineated by the dotted white lines. Higher color scale value corresponds to higher field enhancement. (a) Cross section that is perpendicular to the plane of incidence. (b) Cross

section that is parallel to the plane of incidence. For viewing purposes, the image in (b) is stretched along the vertical direction.

**Fig. 8.** Distribution of the maximum intensification within the silica layers in the defective multilayer coating film for various cone angles and s-polarization light irradiation at a series of incidence angles. (a) 2-D column plot. The red dotted circle indicates that a  $30^\circ$  conical pit generates the least amount of field intensification on average for all incidence angles. The color-box legend indicates the angle of incidence. (b) Contour plot. The blue line indicates that light intensification in mitigation sites is minimized when the cone angle and the incident angle are matched. The color-box legend represents the magnitude of intensification.

**Fig. 9.** Distribution of the maximum intensification within the silica layers in the defective multilayer coating film for various cone angles and p-polarization light irradiation at a series of incidence angles. (a) 2-D column plot. The red dotted circle indicates that a  $30^\circ$  conical pit generates the least amount of field intensification on average for all incidence angles. The color-box legend indicates the angle of incidence. (b) Contour plot. The blue line indicates that light intensification in mitigation sites is minimized when the cone angle and the incident angle are matched. The color-box legend represents the magnitude of intensification.

**Fig. 10.** Electrical field intensity distribution within multilayer coating layers at the presence of a  $15^\circ$  conical pit with a smooth edge (a) and rough edge (b). Beam irradiated at  $45^\circ$  from surface normal. Domain dimension:  $90\ \mu\text{m} \times 4.963\ \mu\text{m}$ . For visualization purposes, all images are stretched along the vertical direction.

**Fig. 11.** Laser damage results on conical pits fabricated by femtosecond laser machining and its correlation to simulation results. Feature size 1 mm conical pit of  $15^\circ$  cone angle. (a) Light

microscope image of fabricated feature before damage test. (b) Light microscope image of conical pit after testing up to  $42 \text{ J/cm}^2$  under irradiation of 1064 nm of s-polarization laser light. (c) Simulation result showing the maximum intensification location for s-polarization light. (d) Light microscope image of conical pit after tested up to  $54 \text{ J/cm}^2$  under irradiation of 1064 nm of p-polarization laser light. (e) Simulation result showing the maximum intensification location for p-polarization light.

**Fig. 1.**

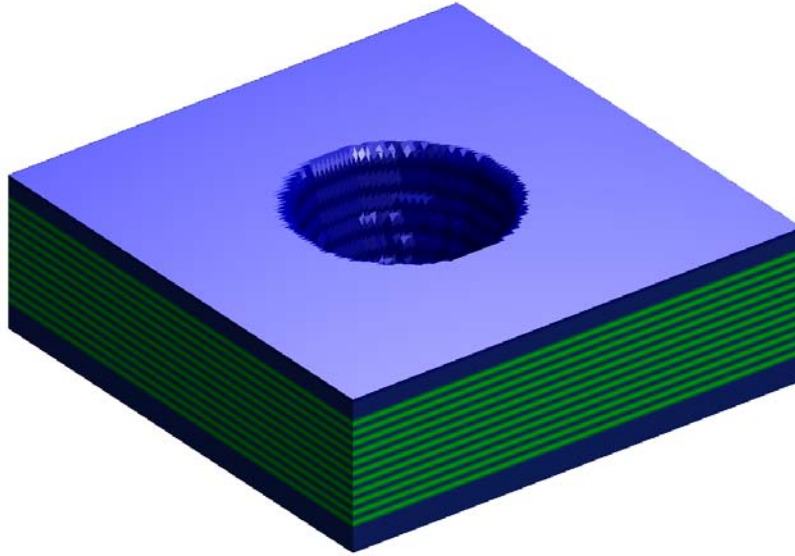
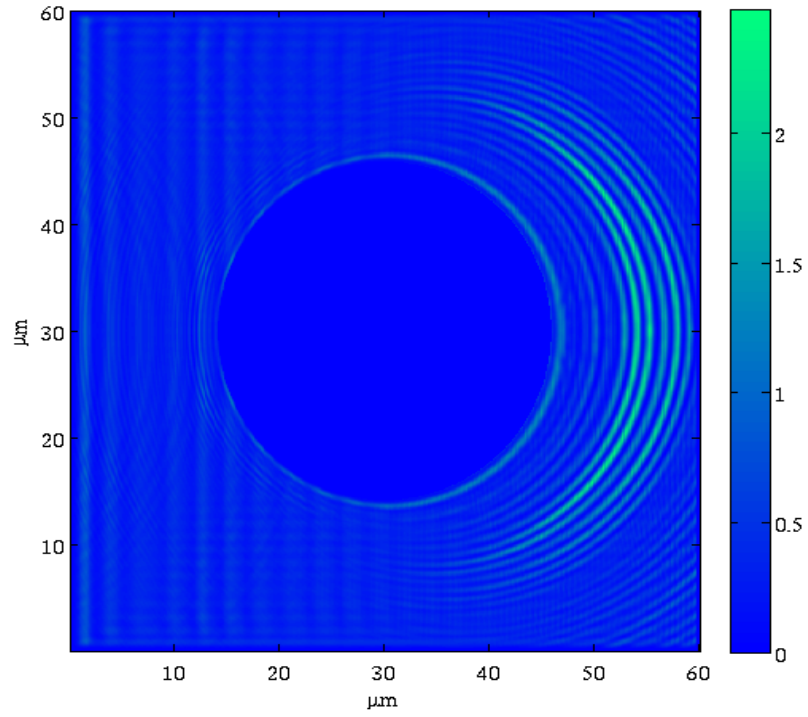


**Fig. 2.**

**(a)**



**(b)**

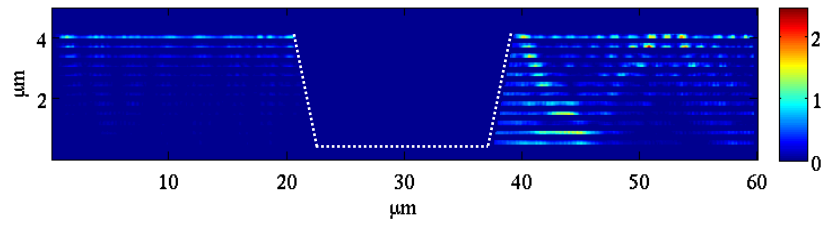
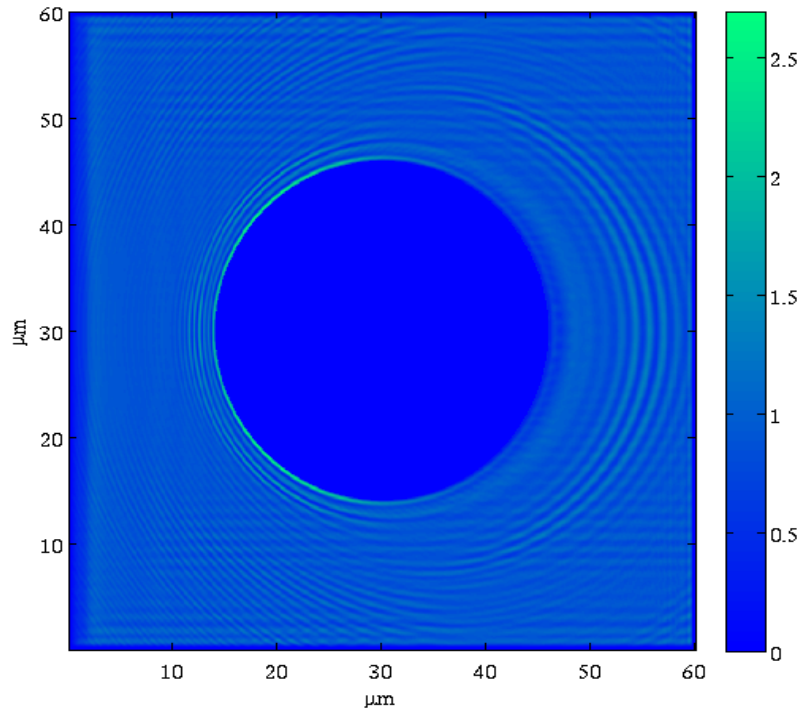


**Fig. 3.**

**(a)**



**(b)**

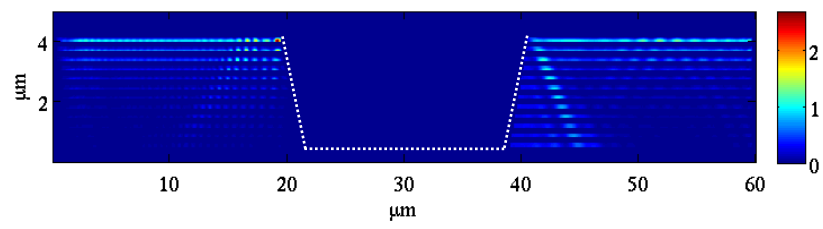
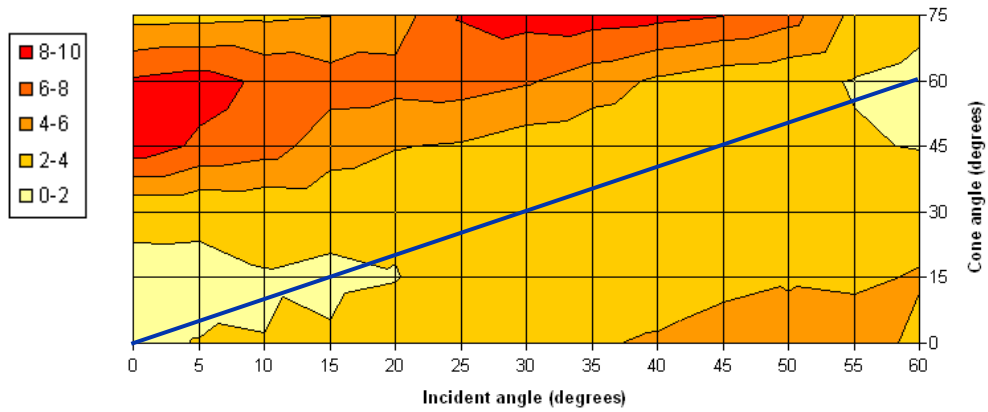
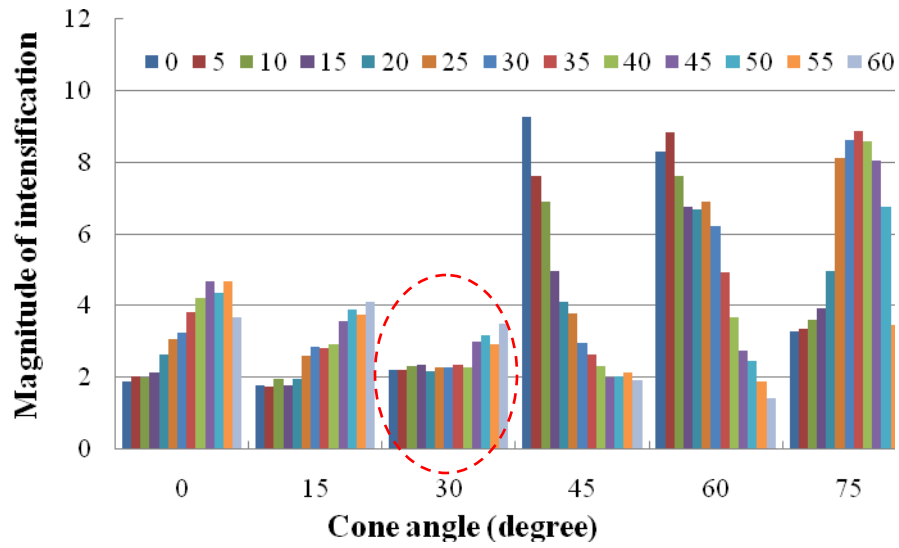
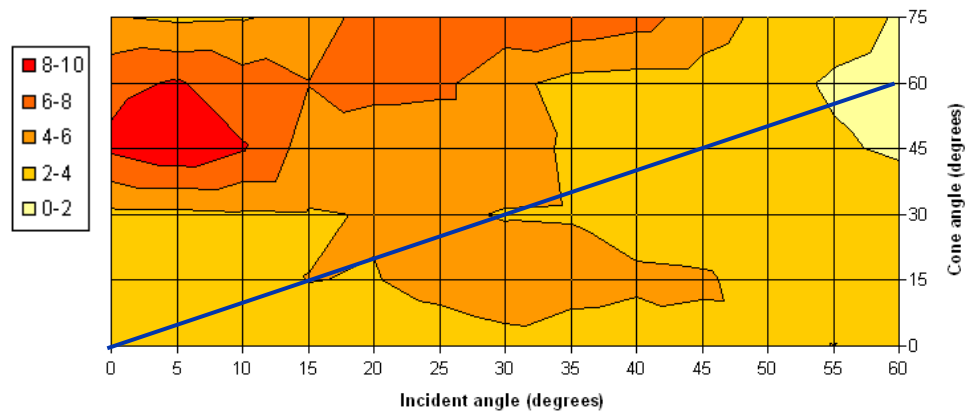
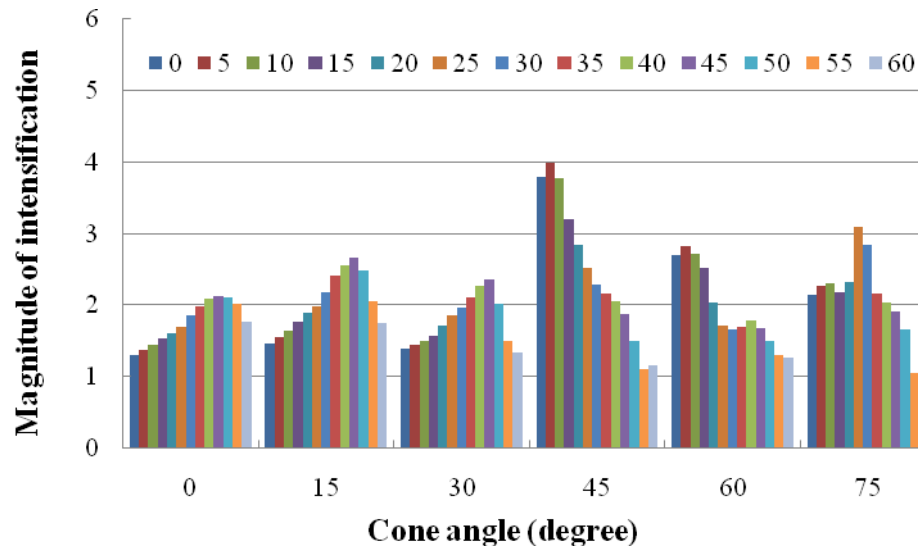


Fig. 4. (S HfOx)



**Fig. 5. (P HfO<sub>x</sub>)**



**Fig. 6.**

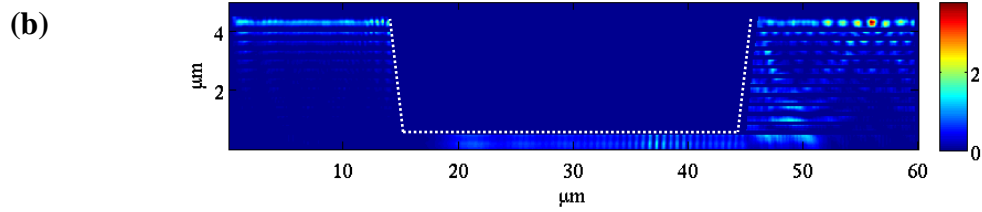
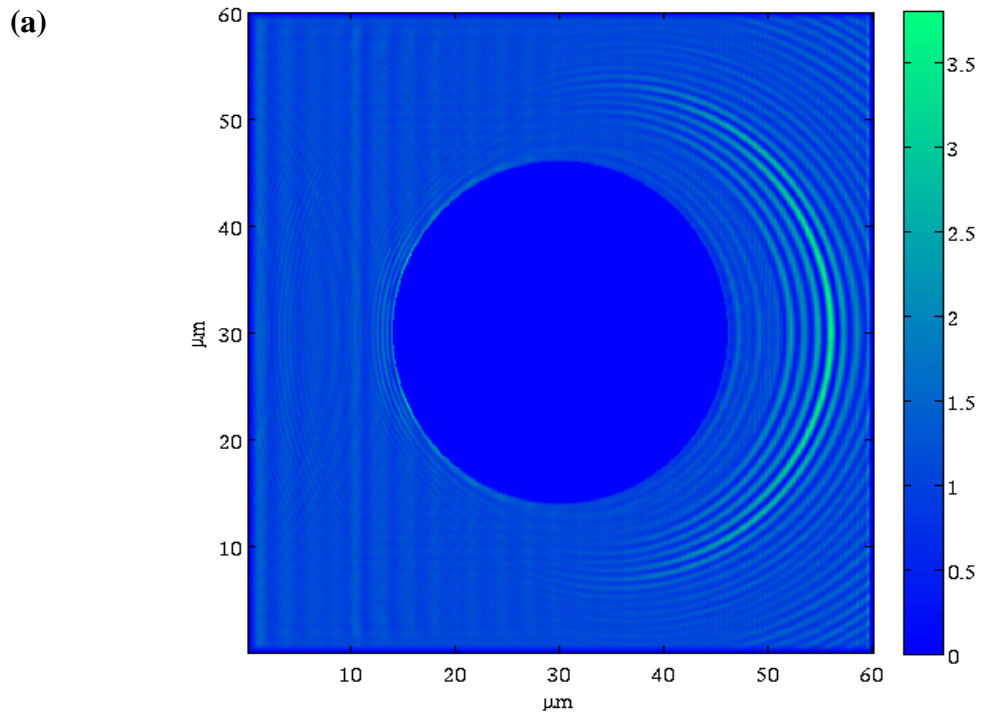
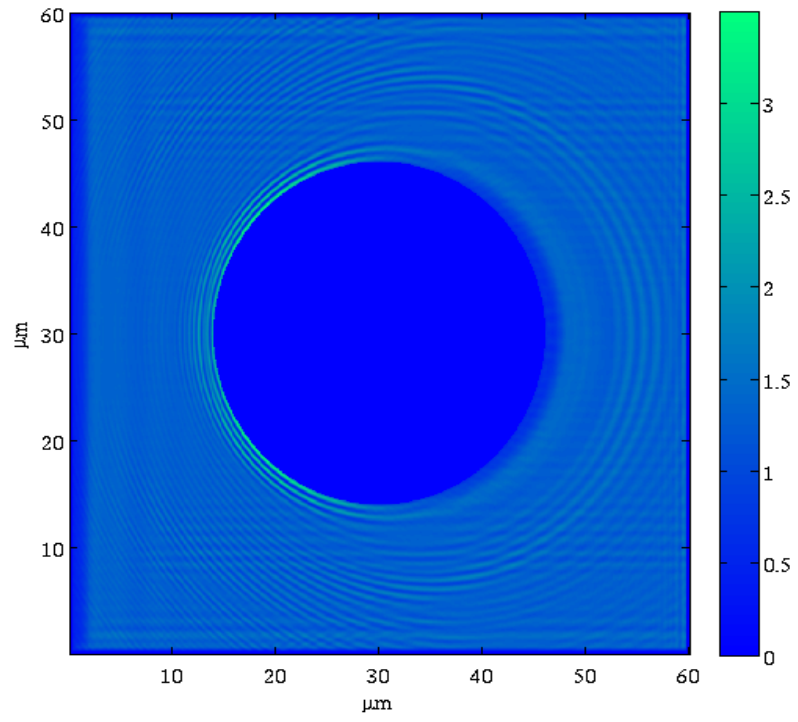


**Fig. 7.**

**(a)**



**(b)**

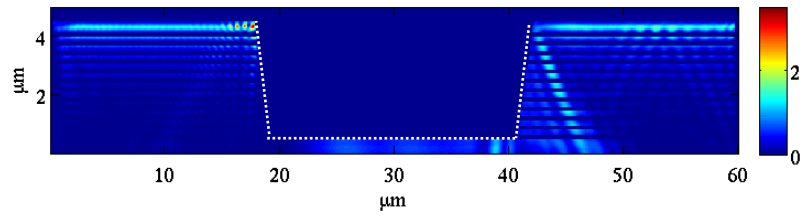


**Fig. 8. (S SiOx)**

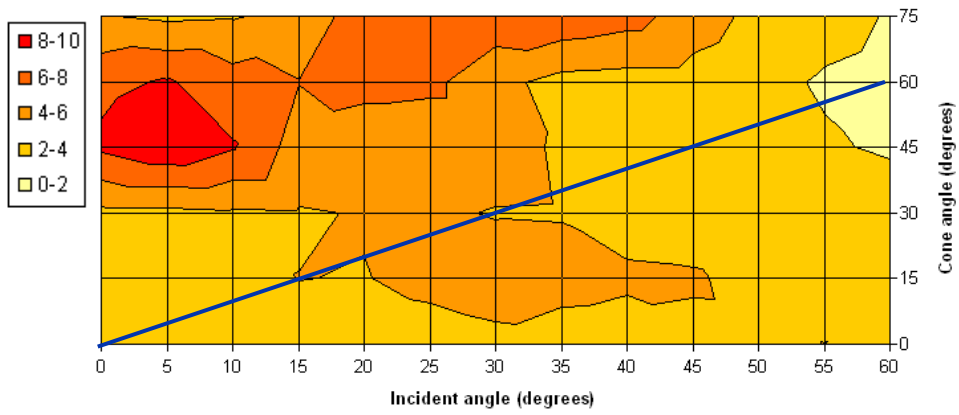
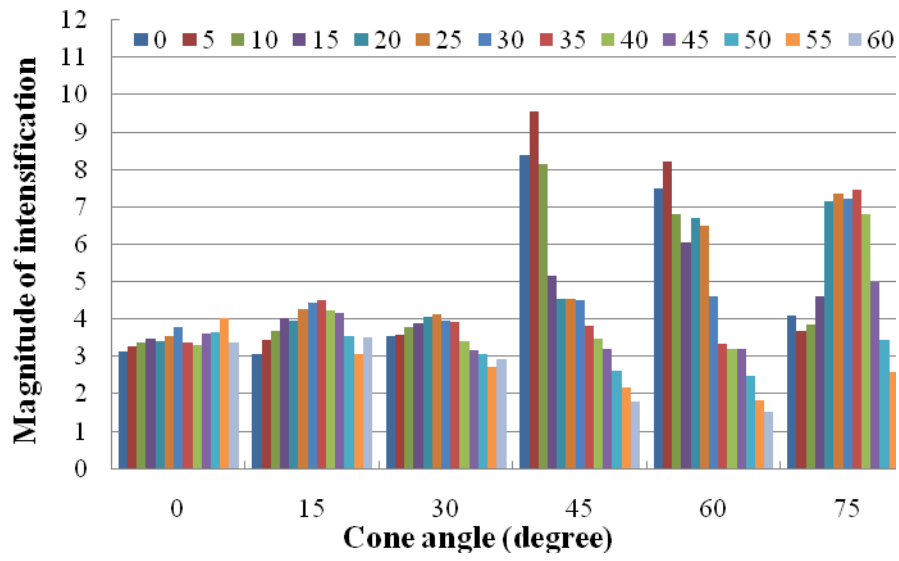
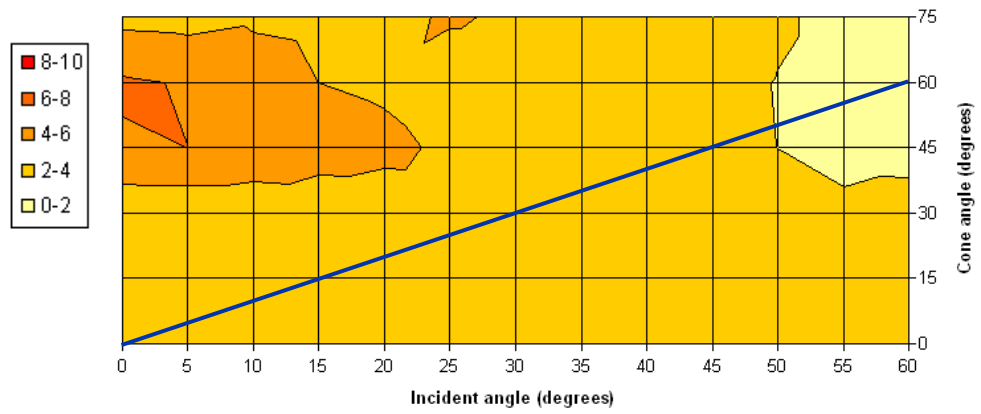
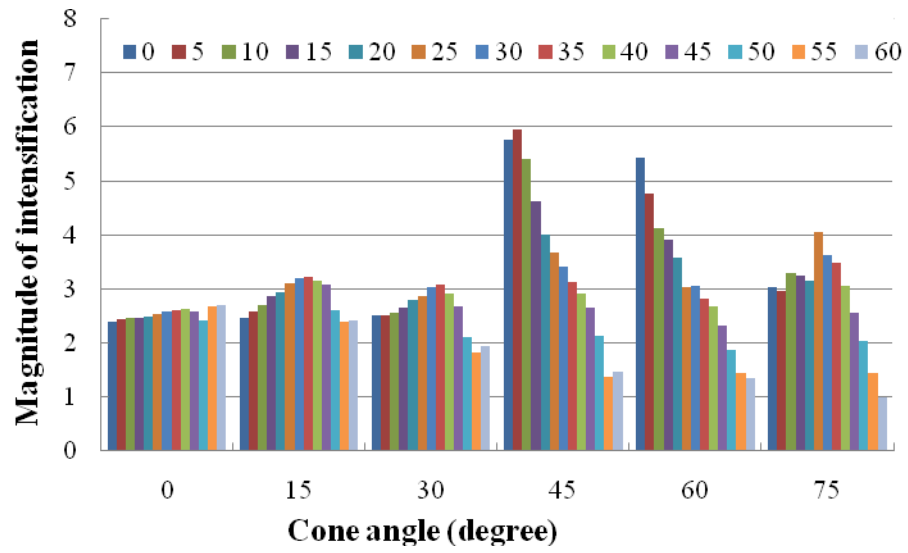
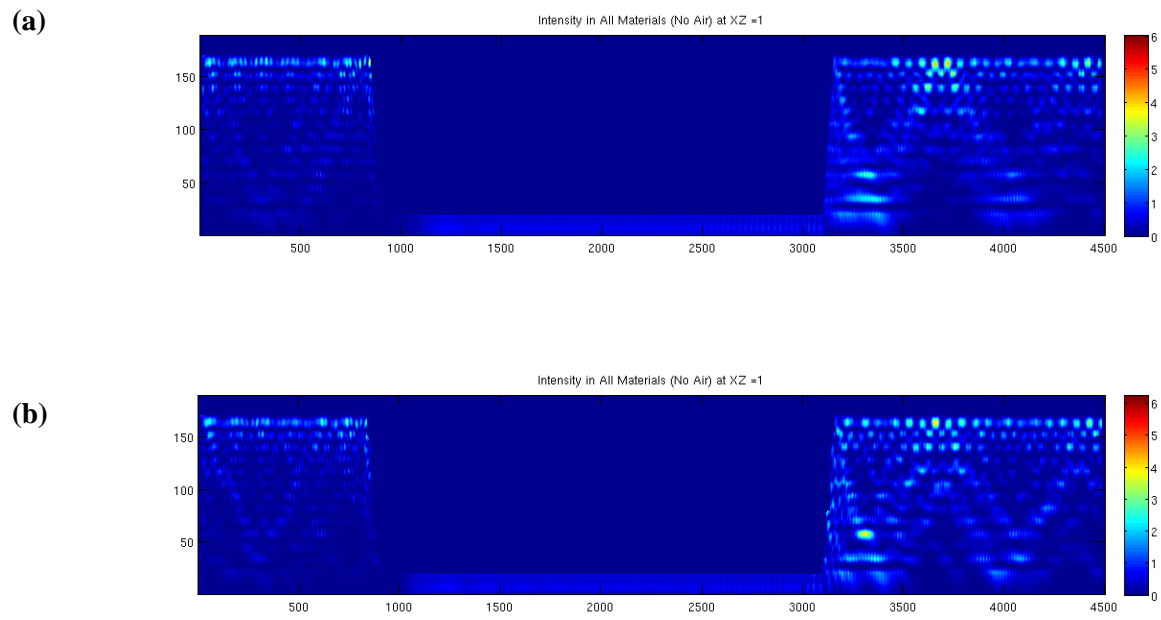


Fig. 9. (P, SiOx)

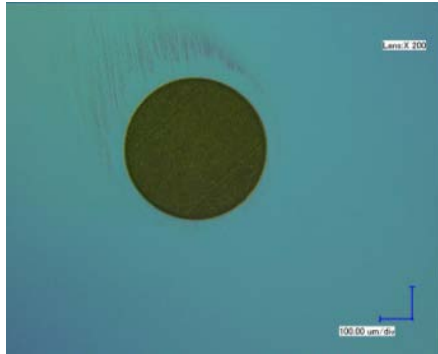


**Fig. 10**

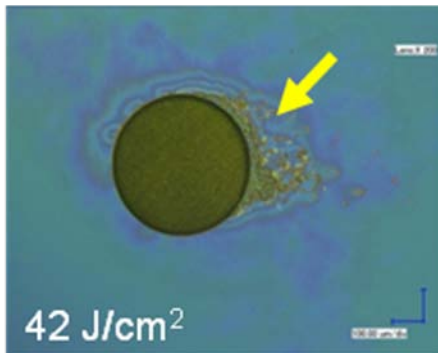


**Fig. 11**

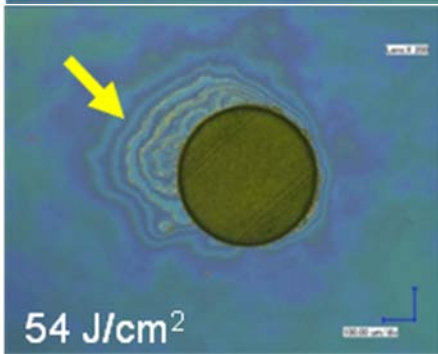
**(a)**



**(b)**

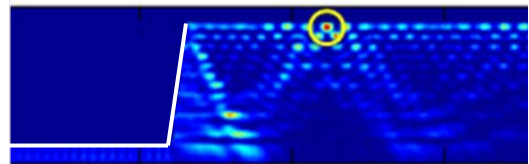


**(d)**



**(c)**

S polarization  $I_{\text{max}} = 3.6$



P polarization  $I_{\text{max}} = 2.6$

